



Science Arts & Métiers (SAM)

is an open access repository that collects the work of Arts et Métiers Institute of Technology researchers and makes it freely available over the web where possible.

This is an author-deposited version published in: <https://sam.ensam.eu>
Handle ID: <http://hdl.handle.net/10985/8545>

To cite this version :

Frédéric GIRAUD, Christophe GIRAUD-AUDINE - Preliminary feasibility study of a speed estimator for piezoelectric actuators used in forging processes - In: 14th European Conference on Power Electronics and Applications (EPE 2011), Birmingham, United Kingdom, 2011-08-30 - Proceedings of the 2011-14th European Conference on Power Electronics and Applications (EPE 2011) - 2011

Any correspondence concerning this service should be sent to the repository

Administrator : scienceouverte@ensam.eu



Preliminary feasibility study of a speed estimator for piezoelectric actuators used in forging processes

Christophe Giraud-Audine

Laboratoire d'Etude des Microstructures et de Mécanique des Matériaux, LEM3, CNRS,
Arts et Métiers Paristech Centre de Metz, 4 rue Augustin Fresnel
57078 Metz, France

Phone: +33 (0) 387-375452

Email: christophe.giraud-audine@ensam.eu

URL: <http://www.ensam.eu>

Frédéric Giraud

Laboratoire d'électrotechnique et d'Electronique de Puissance, L2EP,
Université Lille 1

59655 Villeneuve d'Ascq, France

Phone: +00 (3) 362-531631

Email: frederic.giraud@univ-lille1.fr

URL: <http://www.univ-lille1.fr>

September 1st 2011

Keywords

<<Piezo actuator>>, <<Self sensing control>>

Abstract

In this paper the feasibility of a speed estimator for a piezoelectric actuator used in a forging process is studied. It is based on a simplified linear model and its robustness is tested using a more complex model that include the hysteresis effects. The preliminary results proves that the concept is feasible despite the non-linearities, provided that some parameters of the actuator are known.

Introduction

Vibration in forging processes

The application of vibrations during forming processes have raised interest since the late 50's. In a pioneering paper, Blaha and Langenecker [1] demonstrated that the load applied to a sample dropped when sinusoidal vibrations were superimposed during tensile tests. This phenomenon is fully recognized in the case of extrusion and drawing by several authors [2, 3, 4, 5]. The case of forging was less studied, but some simulation results and reduced scale experiment showed the same trends [6, 7] in the case of the setup presented on Fig. 1 (a). More recently it was theoretically and experimentally demonstrated that in the plastic domain the dominant parameter is the relative speeds of upper die moving at constant speed and the lower die which is animated by the vibration [8]. Such an effect is illustrated on Fig. 1 (b). The upper curve is the forging load without vibrations, then in decreasing order the filtered load curves for sine and triangular waveforms appear. Substantial reduction of the force is obtained with the last waveform. The specifications for the vibrations are :

- high forces (up to 6.10^3 kN)
- small displacement ($40\mu\text{m}$)
- speed up to 5 mm.s^{-1}

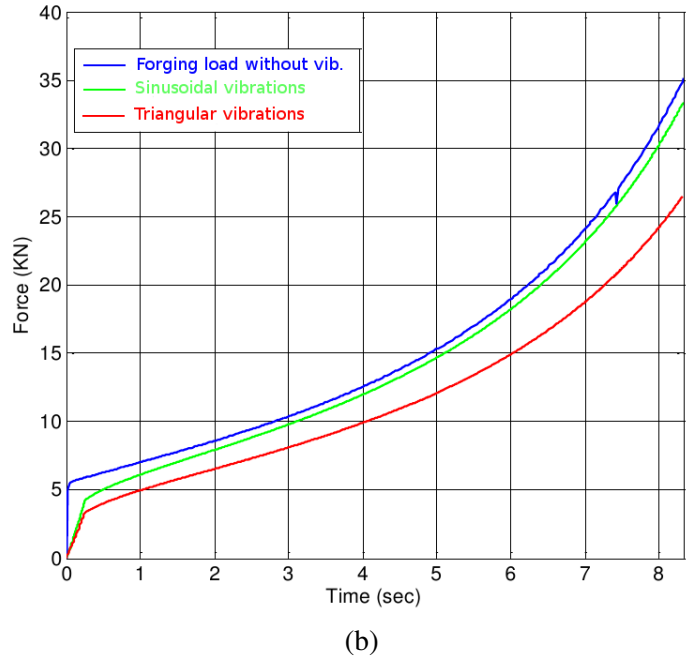
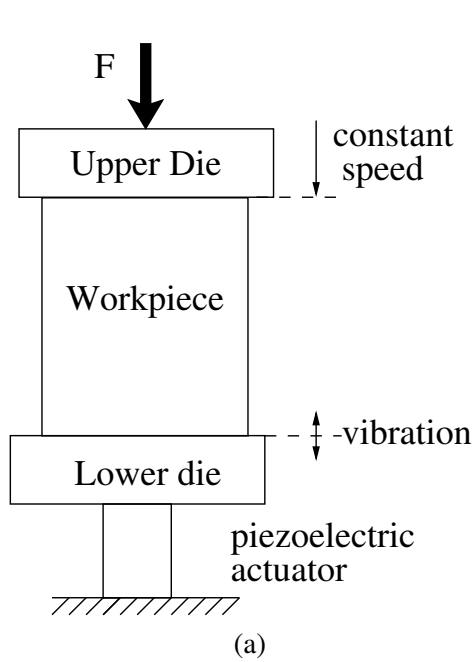


Figure 1: Vibrations assisted forging : (a) schematic of the process (b) Effects on the forging load

- nearly sawtooth like displacement waveform

therefore piezoelectric actuators seem well suited for this application, however some issues need to be addressed.

Scope of the study

The benefit of the vibrations is theoretically maximized in the case of sawtooth displacement waveform applied to the vibrating die. Obviously, this can only be approximated, and in practice, it is realized by imposing piecewise constant speed profile which alternatively take high and low values with a controlled duty ratio. However, two problems appear :

- the piezoelectric actuator present hysteresis and creep nonlinearities
- the forging loads are non linear and vary during the process

Hence closed loop control must be implemented in order to follow the specified speed waveform. On the other hand, in order to meet the load capability requirement, several piezoelectric actuators must be used but the cost of speed sensors for each actuator is totally unacceptable. One possibility which is currently investigated is to estimate the speed using measurement of the currents and voltages applied to the actuators.

Outline of the paper

In this paper we will address the feasibility of such an estimator. Considering the cost involved, it is necessary at this stage to validate the concept using simulations. Therefore, models with different degrees of accuracy have to be developed and implemented. First, a linear model of the actuator will be considered. On this basis, using a macroscopic energetic representation and thanks to the simplicity of the model, it is inverted and the estimator is derived. Second, in order to discriminate and adjust the relevant parameter of the estimator, and test it against the non-linearities of the actual actuator, a more complex model, able to capture the non-linearities is developed based on the Preisach model for voltage and displacement as function of the electrical charges. The model was identified on an actuator using a simple procedure which is one of the interesting features of the proposed model. Finally the estimator is tested and it will be shown that speed is correctly estimated. The limitation will also be explained in the light of the model.

Linear model of the actuator

Linear constitutive equation of piezoelectricity

The piezoelectric actuator (PEA) convert electrical energy into mechanical energy. This process can be modelled by using linear constitutive equations, as those proposed in [9]. In fact, two equations can be introduced in 1, in order to describe the mechanical and the electrical behaviour of a piezo material.

$$\{S\} = [s^E]\{T\} + [d]\{E\} \quad \{D\} = [d]\{T\} + [\epsilon^T]E_k \quad (1)$$

where $[d]$ is the Piezoelectric constant matrix, $[s^E]$ is the elastic compliance constant, $[\epsilon^T]$ is the Permittivity component, $\{T\} = \{T_{11} T_{22} T_{33} T_{12} T_{13} T_{23}\}$ is the stress vector, $\{S\} = \{S_{11} S_{22} S_{33} S_{12} S_{13} S_{23}\}$ is the strain vector, $\{E\} = \{E_1 E_2 E_3\}$ is the electric field, and $\{D\} = \{D_1 D_2 D_3\}$ is the electric displacement.

System modelling

The system (Fig. 2) considered in this section consists in the piezoelectric actuator (PEA), which polling direction is aligned with axis z , attached to the mechanical load modeled by a mass M (representing the weight of the die) and the forging load F_r . The force applied by the mass to PEA upper end ($x = L$ where L is actuator's length) is F while the lower end is fixed. Two electrodes are bonded at $x = 0$ and $x = L$. The cross section of the PEA is noted A . According to this system's description, z is then a symmetry

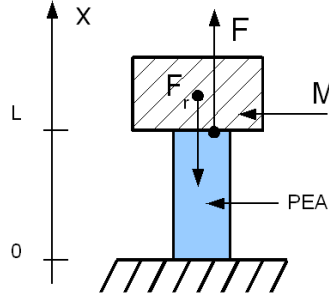


Figure 2: The Piezoelectric actuator and the load M

axis. We will then note $\{E\} = 0, 0, E_3$, leading to $E_3 = \frac{V}{L}$, and we have $F = -T_{33}A$. So, equations 1 reduce to :

$$S_{33} = s_{33}^E T_{33} + d_{33} E_3 \quad D_3 = d_{33} T_{33} + \epsilon_{33} E_3 \quad (2)$$

Finally, the total expansion W of the PEA can be derived from the expression of S_{33} of equation 2 by $W = \int S_{33} dz$, leading to:

$$W = (s_{33}^E T_{33} + d_{33} E_3)L = -\frac{s_{33}^E L}{A} F + d_{33} V \quad (3)$$

The force F produced by the PEA can now be deduced from the voltage V across the electrodes, and the actual displacement of the actuator by:

$$F = K_F V - K_s W \quad (4)$$

with $K_s = \frac{A}{L s_{33}^E}$ and $K_F = \frac{A}{L s_{33}^E} d_{33}$. Moreover, the total amount of charge on an electrode is calculated from 2 and $Q = \iint D_{33} dx dy$:

$$Q = d_{33} T_{33} A + \epsilon_{33} E_3 A = -d_{33} F + \epsilon_{33} \frac{A}{L} V \quad (5)$$

Taking into account 4, 5 is revised into 6 in order to remove F and introduce K_F again:

$$Q = C_b V + K_F W \quad (6)$$

where $C_b = (\epsilon_{33} \frac{A}{L} - d_{33}^2)$ is the blocked capacitance of the PEA.

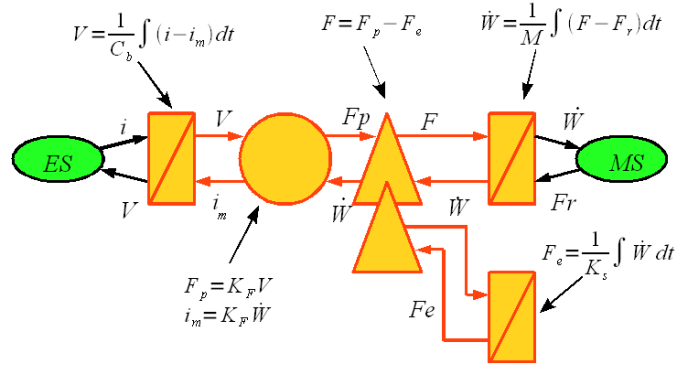


Figure 3: Energetic Macroscopic Representation of the system

These equations have to be re-organized to produce a causal modelling of the system in order to deduce by inversion the equations of a force estimator. To achieve that, we only consider integral causality, avoiding the use of derivative in our equations. From equation 6, we can then write that the voltage across the PEA is obtained from the flowing current into the device i by:

$$V = \frac{1}{C_b} \int (i - i_m) dt \quad (7)$$

with $i_m = K_F \dot{W}$, also called the motionnal current of the PEA. We also define two internal variables F_p , such as $F_p = K_F V$ and F_e , such as $F = F_p - F_e$. It is then obvious from equation 4 that:

$$F_e = K_s W = K_s \int \dot{W} dt \quad (8)$$

Finally, the load dynamic is given by equation 9:

$$\dot{W} = \frac{1}{M} \int (F - F_r) dt \quad (9)$$

This modelling is then represented using the Energetic Macroscopic Representation (EMR). EMR highlights energy storage in the system using crossed out rectangles, in the case at hand :

- kinetic energy in the load M ,
- electric energy in the piezomaterial and the blocked capacitance C_b ,
- elastic energy in the piezomaterial due to K_s .

It also highlights the electrical to mechanical energy conversion process, symbolized by a disk. We found that the voltage V is transformed into an internal force F_p , and in turn, the velocity of the load \dot{W} produces a motionnal current i_m which is an electrical reaction to the mechanical action. Based on this causal modelling, a velocity estimator is described in the following section.

Velocity estimator

The velocity estimator is found by inverting the reaction chain (corresponding to the lower path) of the EMR depicted in figure 3. By this way, it appears that estimation of \dot{W} is more or less an estimation of i_m ; thus equation 7 have to be inverted. But direct inversion of a causal equation leads to a derivative relationship between the estimated motionnal current \tilde{i}_m and voltage V and current i : $\tilde{i}_m = i - C_b \frac{dV}{dt}$. This derivative may brings measurements problems, because high frequency measurement noise of V is then amplified. To reduce this problem, we used an other approached. This approached, described in [10], consists in controlling a virtual capacitance C_b by the estimated current \tilde{i}_m . This is presented in figure 4. The velocity estimator consists in:

A virtual capacitance:

$$V_{est} = \frac{1}{C_b} \int (i - \tilde{i}_m) dt \quad (10)$$

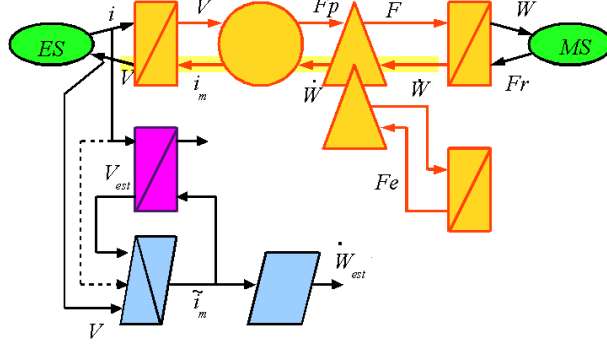


Figure 4: Energetic Macroscopic Representation of the velocity estimator; estimator's path is highlighted in yellow

A voltage regulator made up with a PI controller with compensation of i :

$$\tilde{i}_m = (K_{vp} + \frac{K_{vi}}{s})(V_{est} - V) + i \quad (11)$$

An electrical to a mechanical conversion:

$$\dot{W}_{est} = \frac{1}{K_F} \tilde{i}_m \quad (12)$$

This estimator has been implemented into a Matlab Simulink model. Properties of the piezomaterial, as well as the Parameters of the PI control are given in table I.

Blocked Cap.	Rigidity	Force factor	Weight
$C_b = 180nF$	$K_s = 300N/\mu m$	$K_F = 5.6N/V$	$M = 10g$

Table I: Main specifications of the piezostack actuator (Piezomechanik Pst 500/10-5/15)

A sinusoidal voltage reference of 150V and 5Hz has been applied on the PEA and is presented in figure 5. The voltage controller was designed in order to provide a closed loop bandwidth of approximately 100Hz which is enough for our application.

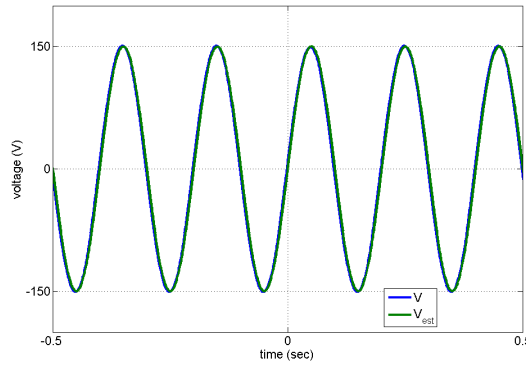
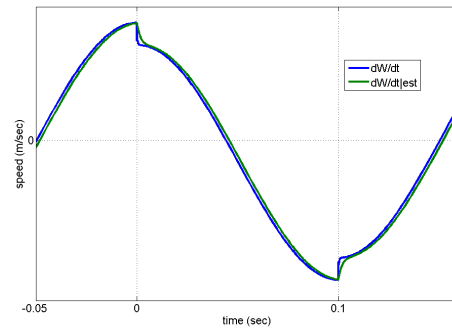
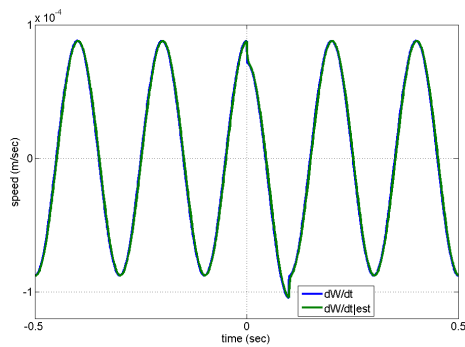


Figure 5: Voltage across the PEA V compared to voltage V_s given by equation 10

The curves depicted in figure 6 and 7 show the velocity of the Piezoelectric actuator compared to the estimated one, where at $t = 0$, F_r increases from 0 to 500N in 0.1 s. Estimated value is consistent with the output of the linear modelling, despite the response time of the motional current estimator. Moreover, this estimator is robust regarding variation of the force F produced by the piezo actuator. The velocity estimator automatically adapts to this loading conditions, after a transient response time.

This velocity estimator relies on a linear modelling of the actuator. However, actual actuator suffer from non linearities in their electrical to mechanical energy conversion process. In order to check the feasibility of a speed estimator based on figure 4, we will use a non linear behavioral modelling on which we will apply the estimator. Before this simulation test to check the capability of our estimator, we also that a force estimator can be deduced from the macroscopic energetic representation.



Force estimator

The force estimator is also deduced from the inversion of figure 4, and proposed in figure 8. The estimated force is calculated from the estimated value of F_p which is deduced from V and $F_p = K_F V$. However, F_e must also be estimated. This force corresponding to elastic strain is an internal force and therefore it cannot be directly measured. However, we can estimate F_e from the estimated value of \dot{W}_{est} and equation 8.

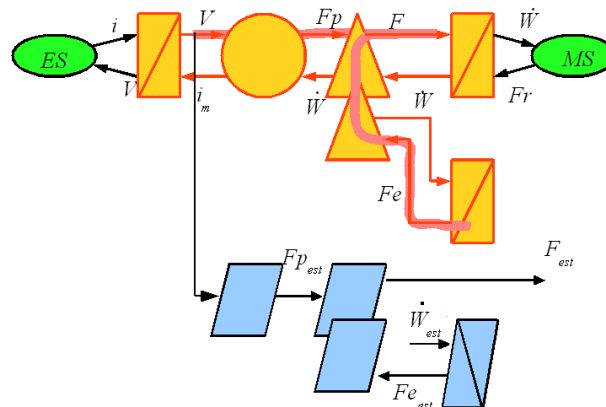


Figure 8: Energetic Macroscopic Representation of the force estimator

Behavioral model

Preisach Model

As mentioned earlier, there is a need for a model which can describe the main non-linear behavior of the piezoactuator. As the frequencies will be low, creep is not to be modeled. On the other hand, the hysteretic nature of the actuator need to be taken into account because it will directly affect the waveforms. To do so, several approaches have been proposed (see [11] for examples of Krasnoselskiĭ-Pokrovskiĭ operator and [12, 13] for Preisach operator based models). Roughly put, these models all relies on the same ingredients, namely :

- a class of hysterons ;
- a weighting function.

Hystérons are operators defined on the input domain which switch between piecewise continuous mapping of the input according to threshold conditions. The most widely used hystérons are :

- the Preisach operator defined by :

$$\Gamma_{(\alpha,\beta)}(\cdot, \gamma_{-1}) : u \in [u_{min}, u_{max}] \mapsto \{-1, 1\} \quad \Gamma_{(\alpha,\beta)}(u, \gamma_{-1}) = \begin{cases} +1 & \text{if } u > \alpha \\ -1 & \text{if } u < \beta \\ \gamma_{-1} & \text{if } \beta \leq u \leq \alpha \end{cases}$$

where γ_{-1} is the previous state of the hysteron.

- the Krasnoselskii-Pokrovskii operator :

$$\begin{aligned} \Gamma_{(\alpha,\beta)}(\cdot, \gamma_{-1}) : u \in \mathbb{R} &\mapsto \mathbb{R} \\ \Gamma_{(\alpha,\beta)}(u, \gamma_{-1}) &= \begin{cases} \max\{\gamma_{-1}, r(u) - \beta\} & \text{if } du > 0 \\ \min\{\gamma_{-1}, r(u) - \alpha\} & \text{if } du < 0 \end{cases} \end{aligned} \quad (13)$$

where the function r is continuous and monotonously increasing, and γ_{-1} is the previous output of the hysteron.

In both case it is assumed that the threshold values verify $\alpha \geq \beta$, thus the set of admissible hysterons belongs to the half plane $\mathbb{P} := \{(\alpha, \beta) \in \mathbb{R}^2 : \alpha \geq \beta\}$. For practical reasons, the input usually belongs to an interval $\mathcal{D} = [u_{min}, u_{max}]$, therefore the triangular plane is considered : $\mathbb{P} := \{(\alpha, \beta) \in \mathcal{D}^2 : \alpha \geq \beta\}$. The output of the hysteresis is the sum over \mathbb{P} of each hysterons output weighted by the weighting function $\mu(\alpha, \beta)$:

$$P_\mu(u, \gamma_{-1}) = \iint_{\mathbb{P}} \Gamma_{(\alpha,\beta)}(u, \gamma_{-1}) \mu(\alpha, \beta) d\alpha d\beta \quad (14)$$

If $\mu(\alpha, \beta) \geq 0 \quad \forall (\alpha, \beta) \in \mathbb{P}$ then the hysteresis is order preserving i.e. given an ordered sequence of inputs $u(t_1) < u(t_2) < \dots < u(t_n)$ will results in an output sequence verifying the inequalities $P(u(t_1), \gamma_0) < P(u(t_2), \gamma_0) < \dots < P(u(t_n), \gamma_0)$.

In this work, a Preisach model was used, and it will now be briefly explained. Only the main properties will be recalled as it is extensively described in literature in the domain of ferromagnetic materials, and it has also been recognized to be useful for piezoelectric actuators [12]. The main interest of this approach is that, along with a very intuitive interpretation, it is easy to implement for a particular set of experimental datas [14]. Indeed, the state of the hysteresis can be understood using a simple geometric interpretation using the Preisach plane (see Fig. a and b). An increasing input will cause all the hysterons

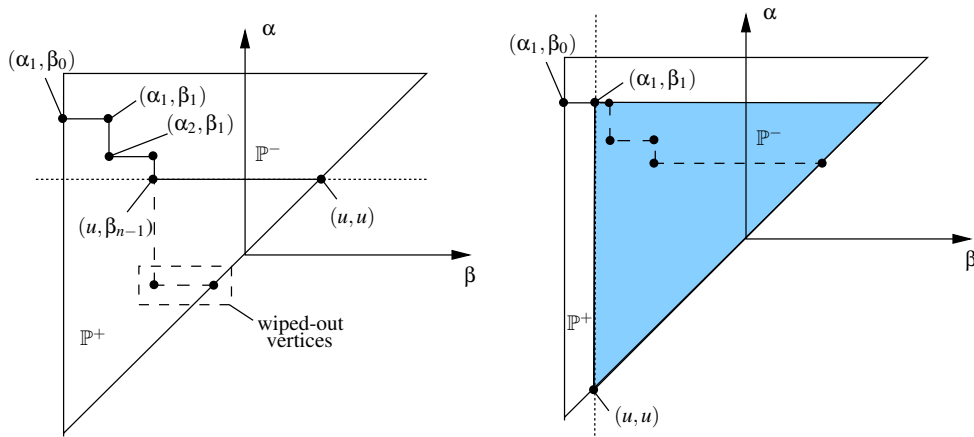


Figure 9: Example of evolutions of the preisach model in the preisach plane : (a) for an increasing input u , (b) for a decreasing output. In both cases wiping-out of vertices occur. The filled triangle is of particular interest for identification as it represents the variation of the output (first order decreasing output)

having threshold $\alpha < u$ to switch to 1 resulting in an horizontal frontier moving upward leaving all hysterons beneath it in the upper state (Fig.9-a). Decreasing the input results in a vertical frontier moving leaving every hysterons at its right in the lower state (Fig.9-b). Note that in the process, vertex can be

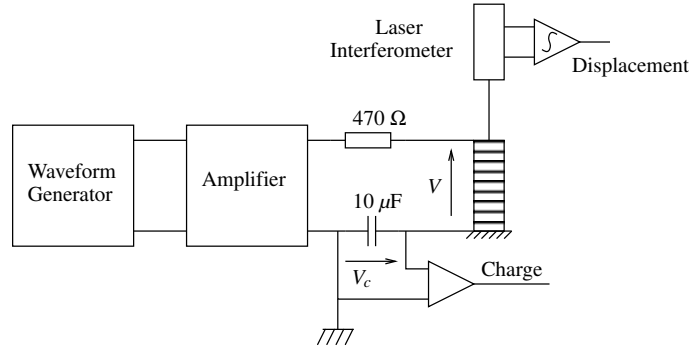


Figure 10: Schematic of the experimental setup

”erased” (wiping-out property) as represented on both example in Fig.9 . Thus, the state of the hysteresis is ”recorded” in the Preisach plane by a staircase-like frontier dividing it into two regions (\mathbb{P}^+ and \mathbb{P}^-) wherein all hysterons have the same state. Each of its vertex represents a pair of local extrema of the input. Let $A = \alpha_0, \alpha_1, \dots, \alpha_n$ be the set of local minima (verifying $\alpha_i > \alpha_{i+1} \quad i \in 0..n-1$), and $B = \beta_0, \beta_1, \dots, \beta_n$ be the set of local maxima, using the linearity of the integral operator, and recognizing that $\alpha_n = \beta_n = u(t)$, Eq. 14 can be rewritten as :

$$\begin{cases} P_\mu(u(t), \gamma_{-1}) = P^- + \sum_{k=0}^{n-1} (T_{\alpha_{k+1}, \beta_k} - T(\alpha_{k+1}, \beta_{k+1})) + T_{u(t), \beta_{n-1}} & \text{if } du > 0 \\ P_\mu(u(t), \gamma_{-1}) = P^- + \sum_{k=0}^{n-1} (T_{\alpha_{k+1}, \beta_k} - T(\alpha_{k+1}, \beta_{k+1})) & \text{if } du < 0 \end{cases} \quad (15)$$

with :

$$T_{a,b} = \int_{\beta=a}^{\beta=b} \int_{\alpha=a}^{\alpha=\beta} \mu(\alpha, \beta) d\alpha d\beta \quad (16)$$

and P^- is the lowest output value, which implicitly suppose that the initial state γ_{-1} is taken at $u = u_{min}$.

From these equations, one can see that in order to calculate the output of the hysteresis, the knowledge of $T_{a,b}$ is enough. A natural way to proceed is to establish a look-up table on a regular grid of the Preisach plane. Values of $T_{a,b}$ in the expressions given by Eq. 15 can then be interpolated according to the variation of the input u . In order to identify, it is usual practice to measure variation of the output of the hysteresis using an input increasing then decreasing (the so-called first order reversal curves). The set of sample values over the Preisach plane is then calculated by :

$$T_{\alpha_i, \beta_k} = P_\mu(\alpha_i, u_{min}) - P_\mu(\alpha_i, \beta_k)$$

Experimental setup

The identification protocol of the PST 150/10-5/15 actuator from Piezomechanik consists in the simultaneous measuring of the charge and the displacement for a selected sequence of voltage. The charge is measured using a Sawyer-Tower circuit. The speed is measured thank to a laser interferometer, the position can then be calculated by integrating the speed signal. The voltage applied follows a progressively increasing triangle waveform such that the slope remains (piecewise) constant during increasing and decreasing phase (such as the one presented in Fig 11-a). This pattern will be useful to measure the first order decreasing curves and ensures that the speed remains fairly in the same range during the test. This is necessary since the piezoelectric hysteresis is known to be rate dependent. It should be noted that in the case at hand, frequency remain below 50 Hz, so this rate dependency is not to be captured by the model.

Model validation

Fig. 11 (c) and (d) illustrate a typical simulation where the voltage applied (Fig. 11 (a)) induces outer and inner loop for the charge and the displacement. The wiping out property and the closing of the loops is verified. In the case of displacement, the integration induces some errors that slightly affect the lower parts of the hysteresis. However, the error is well below the precision required, and it can be seen that the model naturally capture the linearity between charge and displacement as shown in Fig. 11(b). To test further, the model, an arbitrary voltage waveform consisting in linearly increasing and decreasing parts

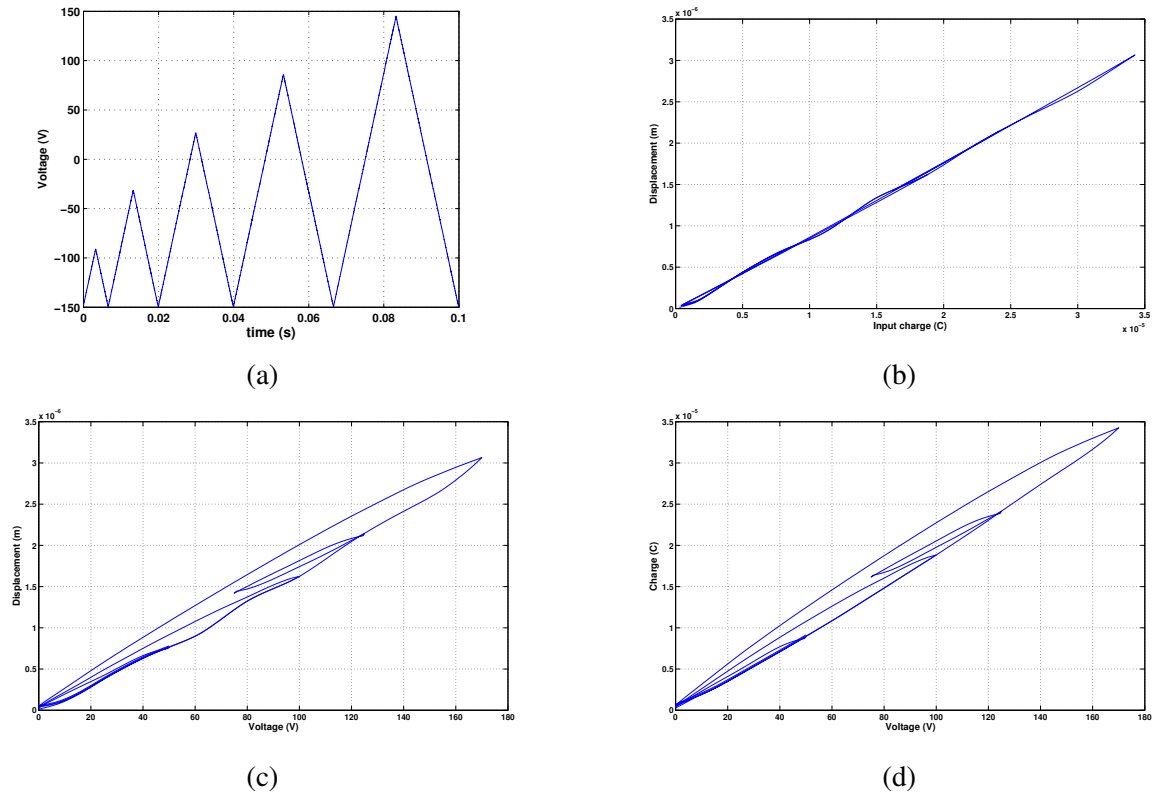


Figure 11: (a) voltage waveform (measured), (b), (c) and (d) show typical simulation results for displacement vs charge, charge vs voltage and displacement vs voltage respectively

was applied to the actuator and the resulting charge and displacement were measured. As Fig. 12 (a) demonstrates, the model is in very good agreement with the measured displacement. On the other hand, Fig. 12 (b) shows that the hysteresis between voltage and electrical charge is less accurate. Actually in the experimental setup, the voltage is imposed by the voltage supply. This guarantees a regular spacing of the voltage measurements, however this is not the case of the voltage of the measurement capacitor. Therefore a resampling of an interpolation of the actual measurements had to be applied introducing errors in the process.

Discussion and future work

The velocity estimator has been applied on the behavioral modelling in order to check whether non linearities such as the one seen Fig. 11 alter the performances of the estimator. In this tests, a sinusoidal current i is applied. After integration, the charge is deduced. These signals are the inputs of the two models. The outputs are compared in Fig. 13

It can be seen that despite non-linearities of the modelling, the real speed is compared to the estimated one. The spikes, appearing on the estimation are due to discontinuities of the variations of the voltage output. These discontinuities can be attributed both to the defaults of the hysteresis modelling and the way it is implemented in simulink.

Future works will aim at experimentally validate the estimator. On the simulation side, the current model of the hysteresis introduce algebraic loops in the simulation. Therefore, a differential model is currently under development.

References

- [1] F. Blaha, B. Langenecker, Tensile deformation of zinc crystal under ultrasonic vibration, *Naturwissenschaften* 42 (1955) 556.
- [2] M. Hayashi, M. Jin, S. Thipprakmas, M. Murakawa, J.-C. Hung, Y.-C. Tsai, C.-H. Hung, Simulation of ultrasonic-vibration drawing using the finite element method (fem), *Journal of Materials Processing Technology* 140 (1-3) (2003) 30–35, proceedings of the 6th Asia Pacific Conference on materials Processing.

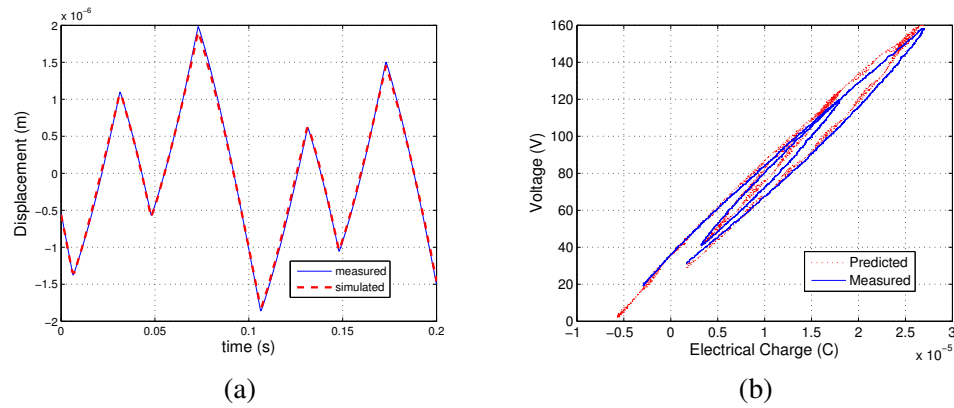


Figure 12: (a) predicted (plain) and simulated (dotted) waveforms (b) Hysteresis of voltage against electrical charge

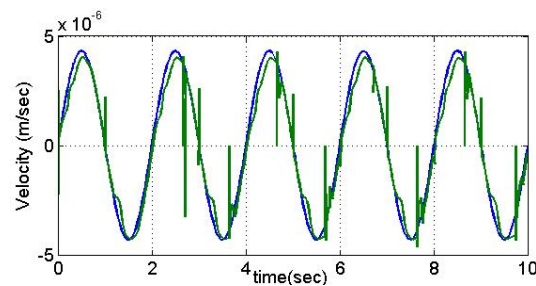


Figure 13: Comparison of the output of a non linear modelling with the output of a velocity estimator based on a linear modelling

- [3] S. Mousavi, H. Feizi, R. Madoliat, Investigations on the effects of ultrasonic vibrations in the extrusion process, *Journal of materials processing technology* 187 (2007) 657–661.
- [4] M. Murakawa, M. Jin, The utility of radially and ultrasonically vibrated dies in the wire drawing process, *Journal of Materials Processing Technology* 113 (1-3) (2001) 81–86.
- [5] K. Siegert, J. Ulmer, Superimposing ultrasonic waves on the dies in tube and wire drawing, *Journal of Engineering Materials and Technology* 123 (2001) 517.
- [6] Z. Huang, M. Lucas, M. Adams, Influence of ultrasonics on upsetting of a model paste, *Ultrasonics* 40 (1-8) (2002) 43–48.
- [7] J. Hung, C. Hung, The influence of ultrasonic-vibration on hot upsetting of aluminum alloy, *Ultrasonics* 43 (8) (2005) 692–698.
- [8] R. Ly, C. Giraud-Audine, G. Abba, R. Bigot, Experimentally validated approach for the simulation of the forging process using mechanical vibration, *International Journal of Material Forming* 2 (2009) 133–136.
- [9] IEEE Standard on Piezoelectricity, ANSI/IEEE Std 176-1987 (1988) 1–74.
- [10] J.-P. Hautier, J.-P. caron, *Systmes automatiques: corus et exercices corrigs*, Ellipses, 1998.
- [11] M. Goldfarb, N. Celanovic, Modeling piezoelectric stack actuators for control of micromanipulation, *Control Systems Magazine, IEEE* 17 (3) (1997) 69–79.
- [12] H. Hu, R. Ben Mrad, On the classical Preisach model for hysteresis in piezoceramic actuators, *Mechatronics* 13 (2) (2002) 85–94.
- [13] H. Hu, H. Georgiou, R. Ben-Mrad, Enhancement of tracking ability in piezoceramic actuators subject to dynamic excitation conditions, *Mechatronics, IEEE/ASME Transactions on* 10 (2) (2005) 230–239.
- [14] A. Bossavit, I. Mayergoyz, E. Corporation, *Computational electromagnetism: variational formulations, complementarity, edge elements*, Vol. 2004, Academic Press San Diego, CA, 1998.